Kinetic modelling of the one-step conversion of aqueous ethanol into 1,3-butadiene over a mixed hemimorphite-HfO_2/SiO_2 catalyst

G. M. Cabello González[1], A. L. Villanueva Perales[1*], M. Campoy[1], J. R. López Beltran[1], A. Martínez[2], F. Vidal-Barrero[1]

[1]Departamento de Ingeniería Química y Ambiental, Escuela Técnica Superior de Ingeniería, Universidad de Sevilla, Camino de los Descubrimientos, s/n. 41092 Sevilla, Spain.

[2]Instituto de Tecnología Química, Universitat Politècnica de València-Consejo Superior de Investigaciones Científicas (UPV-CSIC), Avda. de los Naranjos s/n, 46022 Valencia, Spain.

* Corresponding author
email: angelluisvp@us.es
Departamento de Ingeniería Química y Ambiental, Escuela Técnica Superior de Ingeniería, Universidad de Sevilla, Camino de los Descubrimientos, s/n. 41092 Sevilla, Spain.

Abstract

A kinetic model for the one-step conversion of ethanol into 1,3-butadiene over a mixed hemimorphite-HfO_2/SiO_2 catalyst has been developed, which, as a novelty, accounts for the effect of water content in ethanol on the performance of one-step catalysts, which is important when designing industrial processes. The model considers the formation of the main reaction products (acetaldehyde, water, hydrogen, 1,3-butadiene, ethene, diethyl ether and 1-butanol) as well as numerous minor products, grouped into three lumps (butenes, heavy compounds (C_{6+}), and oxygenated compounds). A network of eight reactions is used to describe this complex reaction system. The rate of each reaction is modelled using a power-law kinetics with a corrective term to capture the effect of water on certain reactions. Experimental data on the effect of water and reaction conditions on the performance of the hemimorphite-HfO_2/SiO_2 catalyst were used for the regression and validation of the kinetic model. The results show that the model can predict well the effect of reaction conditions and water content in ethanol on the formation of major and minor compounds, except for butenes and heavy compounds. The modelling approach to build the kinetic model is expected to be valid for any other one-step catalyst.

Keywords: 1,3-Butadiene, ethanol, kinetics, water, Lebedev

Nomenclature

A	rate constant at reference temperature (mol/g h $bar^{\Sigma ni}$)
a	model parameter for water corrective term
Ac	acetaldehyde
BuOH	1-butanol
C	total number of compounds
D	reactor diameter
DFT	density-functional theory
DRIFT	diffuse reflectance infrared Fourier transform spectroscopy
e	residual
Ea	activation energy (kJ/mol)
EtOH	ethanol
F_k	mole flow rate of compound k (mol/h)
J	jacobian matrix of parameters
L	reactor length
m	exponent of the water corrective term
n	reaction order
N	total number of tests
Ndf	number of degrees of freedom
NR	number of reactions in the kinetic model
p	number of parameters
P	total pressure (bar)
P_k	partial pressure of compound k (bar)
r	reaction rate (mol/h g)
R	ideal gas constant (8.314 J/mol K)
S	objective function
t	Student's t-distribution
T	reaction temperature (°C or K)
V	covariance matrix of model parameters
W	mass of catalyst (g)
Wc	water mass content in ethanol feed (wt %)
WHSV	weight hourly space velocity (h^{-1})

Subscripts/ Superscript

i	reactions
j	experiments
k	compounds
r	parameters

Greek letters

α	significance level
σ	standard deviation
θ	model parameters
υ	stoichiometric coefficient

1. Introduction

1,3-Butadiene is an important feedstock for the manufacture of several chemicals and materials such as styrene-butadiene rubber, polybutadiene rubber, acrylonitrile butadiene styrene resins, styrene butadiene latex, adiponitrile and nitrile rubber [1–3]. Presently, 1,3-butadiene is a by-product of ethene production by steam cracking of naphtha and, therefore, its production is not sustainable. New environmental policies [4,5] have fostered the search for new routes in order to replace fossil-oil derived products with bioproducts [6–8]. For the production of 1,3-butadiene, catalytic conversion of bioethanol into 1,3-butadiene raises as an attractive route since bioethanol is largely available and it can be cost-efficiently produced from a variety of renewable biomass and wastes [1,9]. Hence, in the last decade, the research of more selective and stable catalysts through a better understanding of reaction mechanisms, the required acid/base feature of the catalyst, the impact of preparation methods and the effect of reaction conditions has significantly increased [3,10]. Unfortunately, despite the great advance in catalyst development, the literature

on kinetic models of the conversion of ethanol into 1,3-butadiene is scarce [11], and more research is necessary for efficient design of industrial reactors.

In the literature, several catalytic pathways have been proposed for the conversion of ethanol to 1,3-butadiene. Gruver et al. [12], after studying the conversion of ethanol over aluminated sepiolite, proposed that 1,3-butadiene was generated by the reaction of ethene with acetaldehyde via a Prins-like mechanism, preceded by the formation of acetaldehyde and ethene by ethanol dehydrogenation and dehydration, respectively. However, no experimental evidence supporting this route has been reported to date. Cavani et al. proposed a different reaction pathway over MgO [13] and MgO-SiO_2 [14] catalysts. Based on results from catalytic tests, DFT calculations and in situ DRIFTS experiments, they proposed that acetaldehyde, formed by dehydrogenation of ethanol, reacts with a surface carbanion, formed by the deprotonation of β-carbon of ethanol, to directly produce crotyl alcohol that further dehydrates into 1,3-butadiene. Taifan et al. criticized this reaction pathway since by DFT calculations they found that the surface carbanion on MgO would preferably form ethene rather than 1,3-butadiene [15]. Furthermore, by in situ DRIFT experiments and DFT calculations, Taifan et al. proposed that over MgO-SiO_2 ethanol was converted into 1,3-butadiene via the Toussaint-Kagan pathway [16], which is explained below. Qi et al. has recently proposed a reaction pathway over a Zn-Y-DeAlBEA catalyst, produced by introducing zinc and yttrium into a dealuminated beta zeolite [17], which has common features with that proposed by Cavani et al. in the sense that 1,3-butadiene is formed by reaction of coadsorbed ethanol and acetaldehyde to produce crotyl alcohol, which finally dehydrates into 1,3-butadiene. They proposed a reaction mechanism based on the structure of the catalyst and kinetic studies and derived an expression for the rate of production of 1,3-butadiene,

but the expression was not tested against experimental rate data. Probably, the most supported catalytic pathway from ethanol to 1,3-butadiene is the Toussaint-Kagan pathway (or aldol-condensation pathway), which comprises the following consecutive reactions: (i) ethanol dehydrogenation into acetaldehyde, (ii) self-condensation of acetaldehyde to crotonaldehyde, (iii) conversion of crotonaldehyde into crotyl alcohol by Meerwein-Ponndorf-Verley-Oppenauer (MPVO) reduction with ethanol, and, finally, (iv) crotyl alcohol dehydration into 1,3-butadiene [11,18–24]. This reaction pathway is not free of criticism: some authors have remarked that important intermediates of this pathway, such as crotonaldehyde and crotyl alcohol, are either not detected or present in a very small concentration in the reaction products, which points that they do not play an important role in 1,3-butadiene production. Other authors state that the reason for this is the fast rate of conversion of these intermediates, which precludes their accumulation [11]. Except for the reaction pathway proposed by Gruver et al., the conversion of ethanol into 1,3-butadiene can be described with two reaction steps: a first step in which ethanol is dehydrogenated into acetaldehyde and a second step in which the mixture of acetaldehyde and ethanol reacts to produce 1,3-butadiene. When both steps take place over a single catalyst, we refer to the Lebedev or one-step process, while if each step takes place independently over different catalysts, we refer to the Ostromislensky or two-step process.

According to the recent review by Pomalaza et al. on reactions and catalysts for the conversion of ethanol into 1,3-butadiene [11], the reaction pathways proposed in the literature may co-exist as complementary pathways to 1,3-butadiene or one of them may prevail under specific reaction conditions. The main point of disagreement between the different reaction pathways is how the C-C bond the between ethanol and acetaldehyde is formed, which results in the C_4-

oxygenated precursor of 1,3-butadiene. They state that even for the Toussaint-Kagan pathway, the most accepted, there are important disagreements and lack of understanding concerning the molecular-level mechanisms of the reactions, particularly on the C-C coupling step (the aldol-condensation of acetaldehyde). The reasons are that the molecular-level mechanism varies depending on the type of catalyst and the high instability of the surface intermediates hinders its determination by observation. This lack of knowledge has precluded the development of mechanistic kinetic models for the conversion of ethanol into 1,3-butadiene and explains why there is a scarcity of studies on the kinetics of the one-step conversion of ethanol into 1,3-butadiene. Next, these studies are briefly commented. Bhattacharyya et al. [18], in 1967, investigated the reaction mechanism over a ZnO/Al_2O_3 catalyst by co-feeding ethanol and some intermediates. The results pointed to an aldol-condensation pathway. They established that the acetaldehyde condensation to crotonaldehyde was the rate-limiting step and estimated the apparent activation energy for the overall conversion of ethanol into 1,3-butadiene. Later, in 2014, Tret'yakov et al. [25,26] proposed the only formal kinetic model of a one-step catalyst ($K_2O/ZnO/\gamma\text{-}Al_2O_3$) published so far. The Toussaint-Kagan pathway was modelled as two consecutive reactions: (i) dehydrogenation of ethanol to acetaldehyde and (ii) reaction of two molecules of acetaldehyde with hydrogen to produce 1,3-butadiene and water, thus, supposing that hydrogen was the reducing agent of crotonaldehyde intermediate instead of ethanol. Prins condensation (coupling of ethene and acetaldehyde to 1,3-butadiene) and dehydrogenation of side-product butene, assumed to be formed from ethene dimerization, were also considered possible routes for 1,3-butadiene production. The formation of other side-products was also included in the model: diethyl ether, from ethanol dehydration, and butanal, from acetaldehyde and ethene. Unfortunately, the rationale for the proposal of the reaction network was not presented. Every reaction was assumed to occur

in consecutive elementary reactions over the different active sites of the catalyst. The rate-limiting step for each reaction was supposed to be the one where C-H bonds were broken. The coefficients of the proposed kinetic equations were estimated by fitting the experimental rates of reaction from catalytic tests in a tubular reactor. Some unusual results were obtained, such as the apparent zero reaction order of the 1,3-butadiene formation steps [11]. Besides, neither the goodness of fit was reported, nor statistical analysis and validation of the model was performed. More recently, Bharadwaj et al. [27] proposed a multiscale modelling approach to separate transport limitations from chemical reactions in order to extract intrinsic kinetic parameters in heterogeneous catalytic systems, enabling the study of the effect of physical properties of the catalyst on its performance. They applied that approach to the conversion of ethanol to 1,3-butadiene over a 1Ag/4ZrO_2/SBA-16 catalyst proposing a simplified two-step reaction scheme where a first reaction accounted for the overall conversion of ethanol to 1,3-butadiene and the second reaction for the deactivation of fresh active sites. The rate constants of the first and second reactions were independently determined by fitting experimental data of steady-state conversion of ethanol in short-duration catalytic test and deactivation data in long experimental runs, respectively. Due to the simple reaction scheme, the kinetic model cannot be used to predict the selectivity of the catalyst at different reaction conditions.

A kinetic model of the conversion of ethanol into 1,3-butadiene should account for catalyst deactivation, the effect of reaction conditions (temperature and pressure) and impurities in the ethanol feed to be used for the design of an industrial process. Regarding the latter, water is the main impurity in ethanol feedstock (the Lebedev commercial process used crude bioethanol (~15 wt% water) as feedstock [28]) but it is also the main side product in the conversion of ethanol into

1,3-butadiene. The content of water in the reactor inlet stream is a key design variable. On one hand, a high water content allows using cheaper aqueous ethanol feedstock and reduces the cost of removing water from unconverted ethanol, but on the other hand, water has an undesirable effect on the performance of one-step catalysts, reducing ethanol conversion while promoting unwanted ethanol dehydration to ethene and diethyl ether [14,29–32]. These effects have also been observed in our previous studies on ethanol conversion into 1,3-butadiene over a hemimorphite-HfO_2/SiO_2 catalyst, prepared as a physical mixture of the zinc silicate hemimorphite ($Zn_4Si_2O_7(OH)_2 \cdot H_2O$) and HfO_2/SiO_2 [33], whose 1,3-butadiene carbon yield is one of the highest reported (~70%)[11]. The reduction of ethanol conversion was ascribed to the blocking by water of Zn^{2+} Lewis acid sites of the hemimorphite, which are active for ethanol dehydrogenation, while promotion of ethanol dehydration was attributed to the transformation by water of the Zn^{2+} sites to Brønsted acid sites. Our results also revealed that water inhibited the generation of heavy compounds, formed by successive aldol-condensation reactions of acetaldehyde. These heavy compounds are related to catalyst deactivation. The inhibition of heavy compounds was ascribed to blocking by water of Hf^{4+}-related Lewis acid sites, active for aldol condensation reactions, resulting in slower catalyst deactivation [33]. Although the effect of water content in the ethanol feed on catalyst performance is important, none of the few kinetic models published so far has considered it.

In an effort to contribute to the development of a viable industrial process for the one-step conversion of ethanol into 1,3-butadiene [34], the aim of this paper is to build, for the first time, a kinetic model of a one-step catalyst that accounts for the effect of water as ethanol impurity on the catalyst performance. For this purpose, the results of previous studies on the reaction pathway in

the conversion of ethanol over the hemimorphite-HfO_2/SiO_2 catalyst (in short, HM-HfO_2/SiO_2) [35] and the effect of water and reaction conditions on the catalyst performance [33] were used.

2. Methodology

A simplified reaction scheme comprising eight reactions, eight chemical species and three lumps was proposed based on the reaction network reported for the HM-HfO_2/SiO_2 catalyst by Cabello et al. [35]. A power-law kinetics was assumed for each reaction and corrective terms were introduced to account for the inhibition or promotion of certain reactions with water. Experimental data from previous studies on the conversion of ethanol to 1,3-butadiene over the HM-HfO_2/SiO_2 catalyst [33] were used for the regression and validation of the kinetic model. The kinetic parameters of the model were estimated by fitting the experimental data based on the maximum likelihood principle. For this purpose, differential mole balance equations in the tubular reactor for the chemical species and lumps needed to be solved. Starting from an initial guess of the kinetic parameters, an iterative loop was performed where the values of the kinetic parameters were estimated by an optimizer and then statistically analyzed, the least significant parameter was removed, and a reduced set of kinetic parameters was returned to the optimizer for further estimation. This loop was performed until all parameters retained in the model were significant. Finally, an analysis of residuals and assessment of prediction of the kinetic model on a validation dataset was performed. Details of the methodology are explained next.

2.1. Catalyst synthesis and catalytic tests

The synthesis of the HM-HfO_2/SiO_2 catalyst was presented in a previous work [35] and it is briefly summarized here. First, the HM and HfO_2/SiO_2 components were separately synthesized and then physically mixed in the appropriate proportions to achieve the desired nominal metal

202 composition (3.0 wt% Hf, 9.3 wt% Zn). The resulting fine powder mixture was pelletized, crushed
203 and sieved. The size fraction between 0.3-0.5 mm was used for the catalytic tests.
204
205 For the regression and validation of the kinetic model, catalytic data from our previous
206 studies on the determination of the reaction network in the conversion of ethanol over the HM-
207 HfO_2/SiO_2 catalyst [35] and the effect of reaction conditions and water content in ethanol on the
208 catalyst performance [33], were used. For the study on the effect of reaction conditions (weight
209 hourly space velocity (WSHV), temperature (T)) and water mass content in ethanol (Wc) a design
210 of experiment was performed where different levels were selected for T (340, 360, 380ºC) WHSV
211 (1.12, 3.6, 6.1, 8, 9.8 h^{-1}, calculated as mass flow of ethanol feed (water-free) divided by the mass
212 of catalyst) and Wc (0, 3.75, 7.5 and 15 wt%). In those studies, short-duration catalytic tests were
213 carried out so that catalyst deactivation was negligible, which was checked by comparing catalyst
214 performance at the beginning and the end of each test. That way, the proposed kinetics in this
215 manuscript does not account for catalyst deactivation.
216
217 Information on the catalytic tests regarding reaction conditions and inlet mole flow rates to
218 the reactor, as well as product outlet mole flow rates, can be found in Tables A.1 and A.2,
219 respectively. In order to estimate the kinetic parameters, 48 catalytic tests were randomly selected
220 (estimation data) while the rest of the tests (test number 7, 19, 22, 24, 29, 33, 39, 50, 51 and 56)
221 were used to validate the model (validation data). The carbon balance error in the catalytic tests
222 was below 10%, except for the reaction conditions at high T and low WHSV, where the high
223 formation of heavy compounds raised the error up to 20%.
224

2.2 Reaction scheme

A simplified reaction scheme (reactions 1 to 8) was proposed from the detailed reaction network reported for the HM-HfO_2/SiO_2 catalyst by Cabello et al. [35], which was elucidated by analysing kinetic curves and feeding reaction intermediate compounds. The reaction scheme accounts for the formation of the main (acetaldehyde, 1,3-butadiene, hydrogen and water) as well as minor (diethyl ether, ethene, 1-butanol, butenes, heavy compounds and other oxygenated compounds) reaction products observed in the catalytic tests. The proposed reaction scheme does not represent the molecular mechanism on the catalyst surface, just the overall reactions from ethanol. With this simple reaction scheme, it is mathematically possible to describe the complex reaction system, as it will be shown later.

$$C_2H_5OH \rightarrow C_2H_4O + H_2 \qquad \text{Reaction 1}$$

$$C_2H_5OH + C_2H_4O \rightarrow C_4H_6 + 2H_2O \qquad \text{Reaction 2}$$

$$2C_2H_5OH \rightarrow \left(C_2H_5\right)_2 O + H_2O \qquad \text{Reaction 3}$$

$$C_2H_5OH \rightarrow C_2H_4 + H_2O \qquad \text{Reaction 4}$$

$$2C_2H_5OH \rightarrow C_4H_9OH + H_2O \qquad \text{Reaction 5}$$

$$C_4H_9OH \rightarrow C_4H_8 + H_2O \qquad \text{Reaction 6}$$

$$\frac{13}{2}C_2H_4O \rightarrow C_{13}H_{10}O + \frac{11}{2}H_2O + \frac{5}{2}H_2 \qquad \text{Reaction 7}$$

$$2C_2H_5OH \rightarrow C_4H_8O + H_2O + H_2 \qquad \text{Reaction 8}$$

The production of 1,3-butadiene from ethanol over the HM-HfO_2/SiO_2 catalyst was found to occur through the Toussaint-Kagan pathway [11], which was modelled as two consecutive reactions: (i) ethanol dehydrogenation to acetaldehyde (reaction 1) and (ii) reaction of ethanol and acetaldehyde to 1,3-butadiene and water (reaction 2). This second reaction is an aggregate of the last three reactions in the Toussaint-Kagan pathway (self-condensation of acetaldehyde to crotonaldehyde, reduction of crotonaldehyde to crotyl alcohol with ethanol and crotyl alcohol dehydration into 1,3-butadiene). The reason of this simplification is that the concentration of crotonaldehyde and crotyl alcohol was very low in the reaction products, which precluded an accurate modelling of these intermediate steps. It should be mentioned that reactions 1 and 2 could also be used to model the production of 1,3-butadiene in the case that it occurred through the reaction of adsorbed ethanol and acetaldehyde molecules, as proposed by alternative reaction pathways, since the stoichiometry of the reaction steps is the same [13,14,17]. Regarding diethyl ether and ethene, it was experimentally found that they were formed by ethanol dehydration [35], so their formation was modelled with reactions 3 and 4, respectively. The reaction pathway of 1-butanol from ethanol over the HM-HfO_2/SiO_2 catalyst was not experimentally studied, but the authors believe that 1-butanol is formed by a Guerbet reaction of ethanol [36], because the catalyst is active for aldol-condensation. Since the first step in the Guerbet reaction is ethanol dehydrogenation, already modelled as reaction 1, an additional reaction, the overall formation of 1-butanol from ethanol (reaction 5), was added to the reaction scheme. Between these two reactions, or any linear combination of them, the kinetics of the Guerbet condensation of ethanol is simply described, an approach successfully applied by Riittonen et al. [37]. On the other hand, it was experimentally verified that 1-butanol dehydrated to butenes (1-butene, *cis*-2-butene, *trans*-2-butene, and isobutene) over the catalyst. This transformation is modelled with reaction 6, where

266 butene isomers were lumped to simplify the modelling. Other lumps were also used to group
267 numerous minor compounds. Thus, compounds with more than six carbons (mostly aromatic) were
268 lumped as heavy compounds. These are believed to be formed by consecutive acetaldehyde aldol-
269 condensation and further dehydrogenation and cyclization reactions [38]. For the sake of simplicity
270 their formation from acetaldehyde was modelled with reaction 7. Diphenyl ketone ($C_{13}H_{10}O$) was
271 chosen as a representative compound for heavy compounds since it was identified as a reaction
272 product [35] and its molecular formula is close to that of the aggregate of all the products
273 considered as heavy compounds. Finally, many minor oxygenated compounds (ethyl acetate,
274 acetone, butanal, 2-ethyl-butanol, etc.) were formed over the catalyst from numerous side
275 reactions. Modelling of all these side reactions is impracticable, so these compounds were lumped
276 as oxygenated compounds, whose average molecular formula is close to that of butanal (C_4H_8O).
277 Both ethanol and acetaldehyde are involved in the formation of the oxygenated compounds. By
278 adding the overall formation reaction of butanal from ethanol (reaction 8) to the reaction scheme,
279 and together with reaction 1, the formation of oxygenated compounds from ethanol and
280 acetaldehyde was indirectly described.

281 **2.3. Kinetic model equations**

282 Due to the present lack of knowledge of molecular-level mechanism of this type of catalysts, as
283 well as the large number of unknown side reactions and intermediates, no attempt was made to
284 model the mechanism of the proposed reactions. Thus, a more practical approach was followed,
285 and a power-law kinetics was assumed for each reaction. As commented in the introduction, water
286 inhibits ethanol dehydrogenation (reaction 1) and aldol-condensation reactions (reactions 2, 5 and
287 7) but promotes ethanol dehydration (reactions 3 and 4). Thus, a corrective term $\left(1+a_i P_{H_2O}\right)^{m_i}$ was

introduced in the power-law kinetics, according to Equation 1, to correct the effect of water on the rate of those reactions:

$$r_i = A_i e^{\left(\frac{-Ea_i}{R}\left(\frac{1}{T}-\frac{1}{T_{ref}}\right)\right)} \frac{\prod_{k=1}^{C} P_k^{n_{ki}}}{\left(1+a_i P_{H_2O}\right)^{m_i}} \quad i = 1....NR \qquad \text{Equation 1}$$

where for each reaction i, r_i is the reaction rate in mol/(g·h), A_i is the rate constant at the reference temperature (T_{ref}=360 ºC) in mol/(g h $bar^{\Sigma nki}$), Ea_i the activation energy in kJ/mol, n_{ki} the reaction order of reactant k in reaction i, T the temperature in Kelvin, P_k the partial pressure of reactant k and P_{H2O} is the water partial pressure along the reactor. The corrective term $\left(1+a_i P_{H_2O}\right)^{m_i}$ includes a_i (bar^{-1}) and m_i as fitting parameters, being $m_i \geq 0$ for reactions 1,2,5,7 and 8, $m_i \leq 0$ for reactions 3 and 4, $m_i = 0$ for reaction 6. The corrective term $(1+aP_{H2O})^m$ in the case of reactions 1,2,5,7 and 8 resembles the adsorption term of a Langmuir-Hinshelwood kinetics. This is on purpose since, from our previous work [33], it is known that the active sites of the catalyst for those reactions are blocked by water adsorption. In this regard, other authors have successfully modelled the kinetic inhibitory effect of water for other reactions and catalytic systems with that type of corrective term [39]. It should be noted that the choice of such corrective term it is also mathematically justified because the inhibitory effect of water cannot be simply modelled in a power-law fashion with a negative reaction order, since it would lead to infinite rates of reaction at the inlet of the reactor for an anhydrous ethanol feed.

The kinetic equations for reactions 1 to 8 are shown in equations 2 to 9.

309

310 $$r_1 = A_1 \cdot e^{\left(\frac{-Ea_1}{R}\left(\frac{1}{T}-\frac{1}{T_{ref}}\right)\right)} \frac{P_{EtOH}^{n_1}}{\left(1+a_1 P_{H_2O}\right)^{m_1}}$$ Equation 2

311 $$r_2 = A_2 \cdot e^{\left(\frac{-Ea_2}{R}\left(\frac{1}{T}-\frac{1}{T_{ref}}\right)\right)} \frac{P_{EtOH}^{n_2} \cdot P_{Ac}^{n_3}}{\left(1+a_2 P_{H_2O}\right)^{m_2}}$$ Equation 3

312 $$r_3 = A_3 \cdot e^{\left(\frac{-Ea_3}{R}\left(\frac{1}{T}-\frac{1}{T_{ref}}\right)\right)} \frac{P_{EtOH}^{n_4}}{\left(1+a_3 P_{H_2O}\right)^{m_3}}$$ Equation 4

313 $$r_4 = A_4 \cdot e^{\left(\frac{-Ea_4}{R}\left(\frac{1}{T}-\frac{1}{T_{ref}}\right)\right)} \frac{P_{EtOH}^{n_5}}{\left(1+a_4 P_{H_2O}\right)^{m_4}}$$ Equation 5

314 $$r_5 = A_5 \cdot e^{\left(\frac{-Ea_5}{R}\left(\frac{1}{T}-\frac{1}{T_{ref}}\right)\right)} \frac{P_{EtOH}^{n_6}}{\left(1+a_5 P_{H_2O}\right)^{m_5}}$$ Equation 6

315 $$r_6 = A_6 \cdot e^{\left(\frac{-Ea_6}{R}\left(\frac{1}{T}-\frac{1}{T_{ref}}\right)\right)} P_{BuOH}^{n_7}$$ Equation 7

316 $$r_7 = A_7 \cdot e^{\left(\frac{-Ea_7}{R}\left(\frac{1}{T}-\frac{1}{T_{ref}}\right)\right)} \frac{P_{Ac}^{n_8}}{\left(1+a_7 P_{H_2O}\right)^{m_7}}$$ Equation 8

317 $$r_8 = A_8 \cdot e^{\left(\frac{-Ea_8}{R}\left(\frac{1}{T}-\frac{1}{T_{ref}}\right)\right)} \frac{P_{EtOH}^{n_9}}{\left(1+a_8 P_{H_2O}\right)^{m_8}}$$ Equation 9

In the kinetic model, the independent variables are temperature and partial pressures while A_i, Ea_i, n_{jk}, a_i, m_i are the parameters to be estimated (39 parameters).

2.4. Estimation of the kinetic parameters

The parameters of the kinetic model were estimated fitting experimental data of the catalyst performance (section 2.1) by applying the principle of maximum likelihood, which under the following assumptions, is equivalent to minimizing an objective function [40,41]. Thus, assuming that errors in the observations are independent, normally distributed, with constant variance for each dependent variable, and that the covariance between dependent variables is negligible, the resulting objective function is the sum of the squared of residuals (*e*) divided by the variance of the experimental error. In the objective function (equation 10), the residuals were calculated as the difference between the experimental (F_{kj}) and estimated ($\hat{F}_{kj}$) mole flow rate at the reactor outlet for each compound k along all experiments j; σ_{kj} is the standard deviation of the experimental error of the mole flow rate of the compound k in experiment j, calculated from, at least, three measurements; *N* is the number of experiments, and *C* the number of compounds. Since C=11 and the estimation dataset comprises N=48 catalytic tests, the total number of experimental data points used in the fitting were 528, resulting in a ratio of 13.5 experimental data points per parameter to be estimated.

$$S = \sum_{k=1}^{C}\sum_{j=1}^{N}\frac{\left(F_{kj} - \hat{F}_{kj}\right)^2}{\sigma_{kj}^2} = \sum_{k=1}^{C}\sum_{j=1}^{N}\frac{e_{kj}^2}{\sigma_{kj}^2} \qquad \text{Equation 10}$$

The mole flow rate of each compound at the reactor outlet was calculated by integrating a set of mole balance differential equations in the reactor (Equation 11), where *W* is the mass of catalyst, F_k the mole flow rate of compound (or lump) *k*, υ_{ki} is the stoichiometric coefficient of each compound *k* in the chemical reaction *i* and r_i the rate of reaction i.

$$\frac{dF_k}{dW} = \sum_{i=1}^{NR} \upsilon_{ki} r_i \qquad k = 1...C \qquad \text{Equation 11}$$

In equation 11, two simplifications were imposed: i) ideal plug flow for the experimental laboratory scale reactor since both the ratio between the length (L) and the diameter (D) of the catalyst bed and the axial Peclet number are much greater than 1 [42]; ii) internal and external mass transfer limitations are absent and the controlling step is the chemical reaction. The latter was confirmed for every catalytic test by studying the Mears criterion and the Weisz-Prater criterion for external and internal mass transfer limitation, respectively, as explained by M.A. Portillo et al. [43] and briefly summarized in the Supporting Information (SI). Thus, the use of a pseudo-homogeneous reactor model is justified.

Starting from an initial guess of the kinetic parameters, an iterative loop was performed to estimate the kinetic parameters. First, an optimization was performed where the kinetic parameters were searched in order to minimize the objective function (equation 10). This optimization was carried out in two steps. In the first step, a Nelder-Mead direct-search algorithm was used to find a point close to a minimum, while in a second step an interior-point algorithm continued the search from that point to the minimum. The parameters estimated by optimization were then statistically analyzed and the least significant parameter for a given confidence level was removed. The optimization was again performed for further estimation, but with a reduced set of kinetic

parameters. This loop was performed until all parameters retained in the model were statistically significant, and there was no need to remove any of them. With this strategy, the use of an excessive number of parameters, and therefore, overfitting, was prevented, improving the generalization capability of the model. In the optimization, the reaction orders were bounded between 0 and 3 since higher reaction orders are unusual.

To establish whether the calculated parameters were statistically significant (different from zero), after each optimization a hypothesis test was conducted for every kinetic parameter (θ_r) (H_o: $\theta_r=0$ versus H_a: $\theta_r\neq 0$), where a parameter is significant if the following condition (equation 12) is met:

$$P\left(-\left(\frac{\hat{\theta}_r-0}{SE_r}\right)<t_{Ndf}<\left(\frac{\hat{\theta}_r-0}{SE_r}\right)\right)=1-pval>1-\alpha \quad r=1\ldots p \qquad \text{Equation 12}$$

being $\hat{\theta}_r$ the estimation of the kinetic parameter under consideration, SE_r the standard error of the estimated parameter, p the number of model parameters, t_{Ndf} the t-student distribution with Ndf degrees of freedom (Ndf=C·N-p), pval the p-value and (1-α) the significance level (set to 95% or α=0.05). Thus, a parameter $\hat{\theta}_r$ is statistically different from zero if pval< α. From the parameters which were found to be non-significant after each optimization, the one with the largest p-value was removed from the model. When all parameters were found significant, the estimation loop finished, and confidence intervals (CI) for the remaining model parameters were calculated according to equation 13:

$$CI(\theta_r) = \hat{\theta}_r \pm t_{Ndf,1-\alpha/2} \cdot SE_r \quad r = 1 \ldots p \qquad \text{Equation 13}$$

where $t_{Ndf,\ 1-\ \alpha/2}$ is the t-student variable defined for Ndf degrees of freedom and a confidence interval (1-α/2). The standard error of each parameter (SE_r) was calculated from the diagonal elements (v_{rr}) of the covariance matrix of the model parameters, V_θ (equation 14). This covariance matrix was calculated from the Hessian matrix H_θ [44] using the Gauss-Newton approximation of the Hessian, according to equation 15:

$$SE_r = \sqrt{v_{rr}} \quad r = 1 \ldots p \qquad \text{Equation 14}$$

$$V_\theta^{-1} = \frac{1}{2} H_\theta \quad ; \quad H_\theta \approx 2\left(J^T \cdot J\right) \quad where \quad J = \left(\frac{\partial e_{kj}}{\partial \theta_p} \right)_{\hat{\theta}} \qquad \text{Equation 15}$$

All calculations were carried out using Matlab® software. The integration of the differential equations along the reactor was accomplished with the ode45 routine. For the minimization of the objective function, the fminsearch function, which implements the Nelder-Mead direct-search algorithm, and the fmincon function, which make use of an interior-point algorithm and allows setting bounds for the parameters, were used. The lsqnonlin function was used to obtain the Jacobian matrix (J) at the minimum by the finite difference method.

It should be noted that, to facilitate the estimation of the kinetic parameters, it is of paramount importance to start the optimization algorithm from a good initial guess of the kinetic parameters. To get a good initial guess of the kinetic parameters, a simplified method was carried

out that assumes constant molar flow along the reactor so that the system of differential equations (equation 11) can be transformed into an algebraic system, and the kinetic parameters to be estimated by non-linear regression. Details of this simplified method are explained in a previous work by M.A. Portillo et al. [43].

3. Results and discussion

3.1. Prediction capability of the kinetic model

The estimated kinetic parameters are shown in Table 1, while the comparison for each compound between the experimental mole flow rates and those predicted by the model is shown in Figure 1. The fitting is good, not only for the most abundant compounds at the reactor outlet (ethanol, acetaldehyde, water, hydrogen, and 1,3-butadiene), but also for most of the minor ones (ethene, diethyl ether, 1-butanol, and oxygenated compound lump). Approximately 90% of the points lie within the ±20% error bands. This result indicates that the chosen reaction scheme includes the most important reactions occurring over the catalyst. Only the fitting of the lumps butenes and heavy compounds is not so good. An obvious reason is that it is difficult to predict an aggregation of multiple compounds that are formed through different reactions by using only one reaction, particularly in the case of heavy compounds. This problem is magnified when trying to model the effect of water on their formation: the kinetic model slightly overestimates the formation of heavy compounds for an aqueous ethanol feed while underestimates it for an anhydrous ethanol feed. An additional difficulty is that there is a relatively large error in the quantification of the heavy compounds in the catalytic tests, which distorts the material balance and therefore, the fitting.

Table 1. Estimated values of the kinetic parameters. Note: N.s=found non-statistically significant.

	A (mol/g h $bar^{\Sigma ni}$)	**Ea** (kJ/mol)	**Reaction order** EtOH	**Reaction order** Ac	**Reaction order** BuOH	**a** (bar^{-1})	**m**
r_1	24.68±0.37	151.95±0.34	2.49±0.08	-	-	999.97±53.56	0.33±0.01
r_2	3.46±0.21	181.67±0.84	1.55±0.01	0.54±0.01	-	22.59±2.99	0.59±0.03
r_3	$(9.64\pm0.42)\cdot10^{-2}$	118.59±8.96	2.49±0.21	-	-	N.s	N.s
r_4	0.24±0.01	190.31±0.73	2.09±0.02	-	-	N.s	N.s
r_5	$(7.64\pm0.18)\cdot10^{-3}$	199.73±1.02	0.32±0.01	-	-	68.81±2.98	0.94±0.02
r_6	0.55±0.06	233.17±1.31	-	-	0.96±0.02	-	-
r_7	4.37±0.46	50.00±6.45	-	2.49±0.11	-	N.s.	N.s
r_8	0.26±0.03	210.53±1.15	0.83±0.02	-	-	908.82±196.89	0.73±0.02

In order to validate the assumptions of the regression model (that the errors follow a normal distribution and have a constant variance [45]), the residuals were analyzed. The standardized residuals are normally distributed (Figure B.1) as they fairly follow the normal-distribution line, so it can be considered that the normality hypothesis is also fulfilled. The homoscedasticity hypothesis (constant variance) was validated by plotting for each compound the standardized residuals against predicted values (Figure B.2). The standardized residuals of the main compounds (ethanol, acetaldehyde, hydrogen, 1,3-butadiene, water, diethyl ether, and ethene) do not follow any trend and also no change is observed in their spread around the zero line as one moves from left to right along the plots. Therefore, the homoscedasticity hypothesis is fulfilled for those compounds. On the other hand, the spread of the residuals of the lumps butenes and heavy compounds follow a downward linear trend. Although for these minor compounds the homoscedasticity hypothesis is violated, it is fulfilled for the major compounds and therefore the model is accepted.

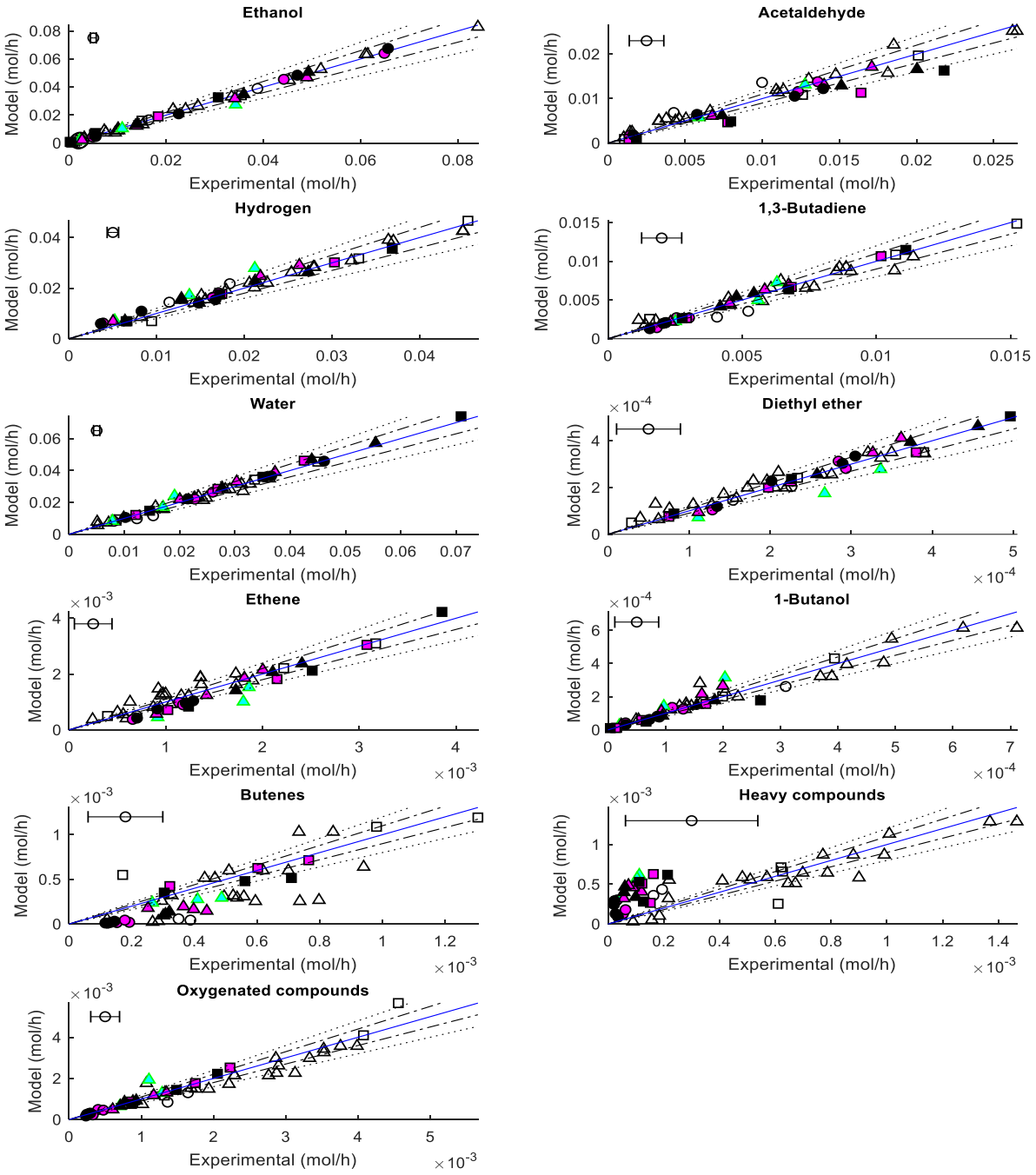

438

439 Figure 1. Parity plots of the experimental and predicted mole flow rates for each compound/lump. (●
440 340°C, ▲360°C and ■ 380°C, symbol color: white 0%w/w water in ethanol feed, green 3.75 wt%,
441 magenta 7.5 wt%, and black 15 wt%); Error bands: 10% (dash-dotted line), 20% (dotted line). For
442 each chemical species, the average uncertainty of the experimental mole flow rates is shown in the
443 upper-left side of the plot.

The validation of the kinetic model was performed by testing it against the experimental data that was not used for the fitting (validation data). Figure 2 compares the predictions of the model against the validation data. The distribution of the points in the parity plots of Figure 2 for each compound is like that in Figure 1, consequently the kinetic model has not been overfitted. Again, most of the points lie within the ±20% error bands, except for butenes and heavy compounds, thus the generalization capability of the model is acceptable.

From the above assessment, it can be concluded that, overall, a good prediction capability of the kinetic model is expected except for some lumps (butenes and heavy compounds). However, these lumps usually comprise less than 10% of the product stream on a mole basis, so only a small error is expected when estimating the overall performance of the catalyst with the help of the kinetic model. Therefore, the kinetic model can be a useful tool in the design of an industrial process for the one-step conversion of ethanol to 1,3-butadiene since it will allow to analyse the impact on process performance of reaction conditions, the use of aqueous ethanol as feedstock as well as the degree of water removal from unconverted ethanol.

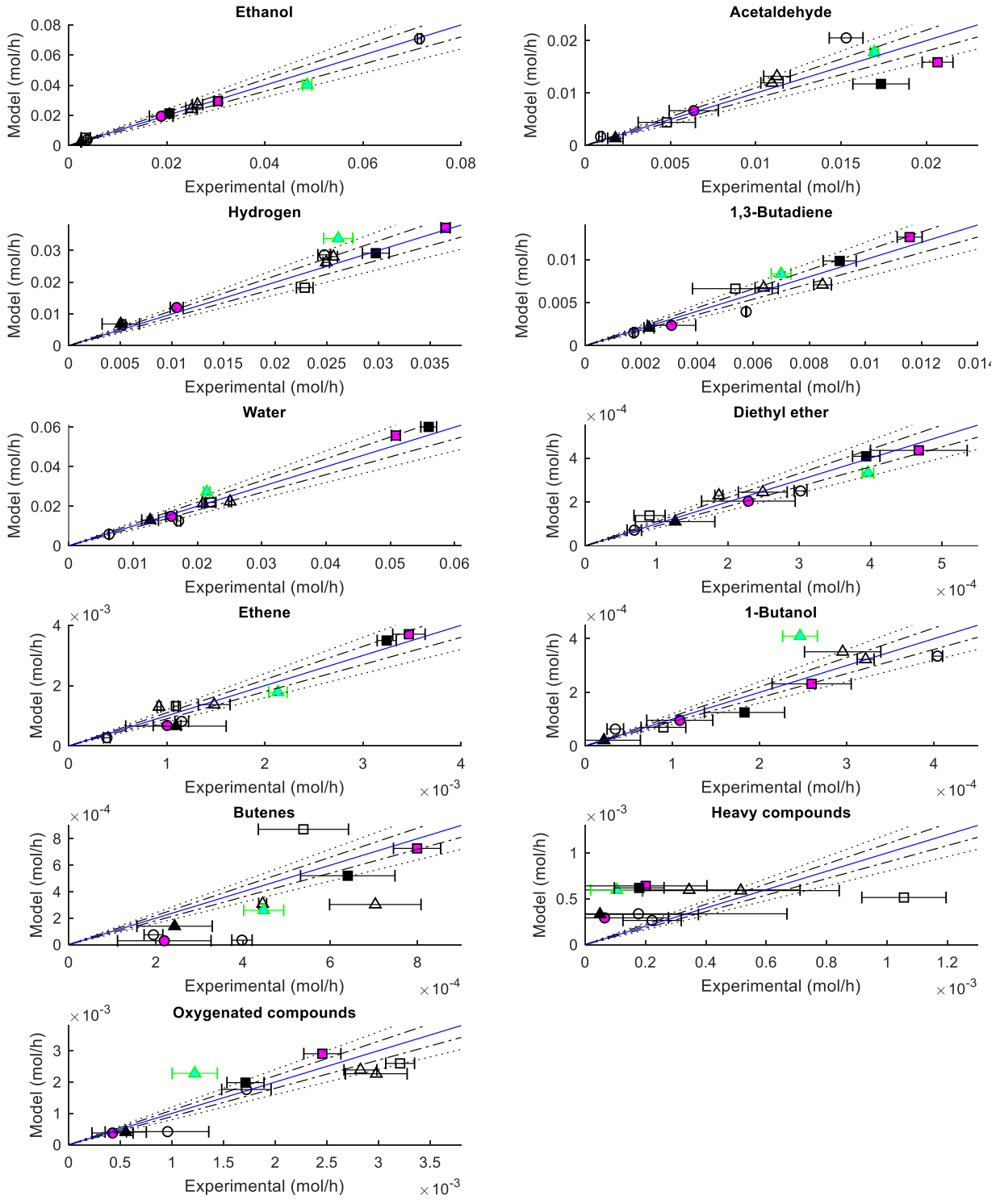

Figure 2. Parity plots of experimental and predicted mole flow rates for the validation data. (● 340°C, ▲ 360°C and ■ 380°C, empty symbols 0 wt% water, cyan 3.75 wt% water, magenta 7.5 wt% water and black 15 wt% water). 10% error band (dash-dot line), 20% error band (dotted line).

3.2. Non-significant kinetic parameters

In the estimation of the kinetics parameters, corrective terms of reactions 3 and 4 (ethanol dehydration to diethyl ether and ethene, respectively), and reaction 8 (formation of heavy compounds from acetaldehyde) were removed from the model as they were found not significant in the statistical analysis. Regarding reactions 3 and 4, their corrective terms were expected to account for the increase in the formation of ethene and diethyl ether when using an aqueous ethanol feed, whose underlying cause was the transformation of Lewis acid sites into Brønsted acid sites by water. The removal of these terms makes us believe that the role of Brønsted acid sites is minor in that matter and that the larger generation of ethene and diethyl ether achieved with aqueous ethanol can be explained by the inhibition of ethanol dehydrogenation (reaction 1), which results in more ethanol available to be converted into ethene and diethyl ether. The inhibition of ethanol dehydrogenation by water can also be the reason why the corrective term of the reaction 8 is unnecessary, because the resulting lower availability of acetaldehyde reduces the formation of heavy compounds.

3.3. Comparison with other works in the literature

There is only one kinetic model for a one-step catalyst available in the literature which was developed by Tret'yakov et al. [25,26] for a $K_2O/ZnO/\gamma\text{-}Al_2O_3$ catalyst. There are important differences between that model and the one reported in the present work in terms of the proposed reaction network and kinetic equations. Regarding the reaction network, Tret'yakov et al. did not perform, to the best of our knowledge, a study of kinetic curves or of any other nature to elucidate it, so it is unknown the rationale behind it. One of the main differences in the reaction network when compared to our work is that they considered Prins condensation and dehydrogenation of

490 butenes as routes for 1,3-butadiene, in addition to the Toussaint-Kagan pathway. This is debatable
491 since dehydrogenation of butenes is thermodynamically unfavored [3] while Prins condensation is
492 thermodynamically less favorable than the Toussaint-Kagan pathway [36]. The importance of
493 these two routes relative to the Toussaint-Kagan pathway in describing the production of 1,3-
494 butadiene over their catalyst is unknown, since their relative contributions were not reported once
495 the kinetic model was regressed. On the other hand, in the present work, the production of 1,3-
496 butadiene was well modelled only with the Toussaint-Kagan pathway, which was demonstrated to
497 occur over the catalyst [35]. In both works, the Toussaint-Kagan pathway is modelled as two
498 consecutive reactions: (i) ethanol dehydrogenation to acetaldehyde and (ii) conversion of two
499 molecules of acetaldehyde to butadiene and water in the presence of a reducing agent (ethanol in
500 the present work and hydrogen in that by Tret'yakov et al.). Regarding the latter, while there is a
501 consensus on the role of ethanol as reducing agent, it is currently under debate whether hydrogen
502 gas can also act as reducing agent. ZnO can perform the heterolytic dissociation of hydrogen, so it
503 could explain why Tret'yakov et al. considered hydrogen as reducing agent but not why they
504 excluded ethanol as such [11].

505 Regarding the kinetic equations, Tret'yakov et al. [25] distinguished three distinctive active
506 sites of the catalyst where the reactions take place. For each reaction, they derived a kinetic
507 equation by assuming a mechanism and a rate-limiting step. An unusual feature of the kinetic
508 model by Tret'yakov et al. is that the reaction order of the butadiene formation steps is zero. Also,
509 the model cannot account for the severe effect of water on the performance of one-step catalysts
510 [14,28,30–33] since water adsorption was not modelled in the kinetic equations. On the other hand,
511 in the present work, a straightforward approach was followed by making use of a power-law
512 kinetics due to the present lack of knowledge of the molecular-level mechanism for one-step

513 catalysts [11]. As explained before, the kinetic model successfully accounts for the effect of water
514 in the reactions by introducing a corrective term in the kinetic equations, and, unlike the model by
515 Treat'yakov et al., the rate of 1,3-butadiene production was found to increase with acetaldehyde
516 and ethanol partial pressures.

517 Finally, the validity and accuracy of the model by Treat'yakov et al. cannot be compared
518 with that presented in this work, since they did not report any statistical analysis. More kinetic
519 studies of one-step catalysts are necessary in the literature, particularly using an aqueous ethanol
520 feed, due to the lack of research in this subject.

521 **4. Conclusions**

522 A kinetic model for the conversion of ethanol to 1,3-butadiene over a hemimorphite-
523 HfO_2/SiO_2 catalyst has been developed, comprising eight reactions, eight chemical species and
524 three lumps in order to account for the formation of the main and minor reaction products formed
525 over one-step catalysts. The novelty of the kinetic model is the consideration of the effect of water
526 content in ethanol on catalyst performance, which is a cornerstone feature if the kinetic model is
527 intended to be used for designing industrial processes using aqueous ethanol as feedstock. The
528 former is achieved by introducing a corrective term in the power-law kinetics of each reaction
529 whose rate is affected by water. Experimental data on the effect of water and reaction conditions
530 on the performance of the hemimorphite-HfO_2/SiO_2 catalyst were used for the regression and
531 validation of the kinetic model. By using statistical analysis, only significant parameters were
532 retained in the model. The results show that the model can predict well the effect of reaction
533 conditions and water content in ethanol on the formation of major and most minor compounds,
534 except butenes and heavy compounds. Thus, the use of lumps simplifies the modelling, but limits

the accuracy of the model. The modelling approach to build the kinetic model is expected to be valid for any other one-step catalyst. Such kinetic model will help to design more efficient processes for production of 1,3-butadiene from bioethanol as it is able to analyze the impact on process performance of reaction conditions, the use of aqueous ethanol as feedstock as well as the degree of water removal from unconverted ethanol.

Further work is necessary to improve the model to account for the decay in catalyst activity by coke deposition. In addition, a more accurate modelling of the formation rate of heavy compounds and butenes could be achieved at the cost of a much more complex reaction scheme.

Acknowledgements

This work has been carried out in the framework of the project "Biobutadiene production from bioethanol" (CTQ2015-71427-R) funded by the Spanish Ministry of Economy, Industry and Competitiveness (MINECO) through the European Regional Development Fund (ERDF).

References

[1] S. Shylesh, A.A. Gokhale, C.D. Scown, D. Kim, C.R. Ho, A.T. Bell, From Sugars to Wheels: The Conversion of Ethanol to 1,3-Butadiene over Metal-Promoted Magnesia-Silicate Catalysts, ChemSusChem. 9 (2016) 1462–1472. doi:10.1002/cssc.201600195.

[2] A.J. Nizamoff, On-Purpose Butadiene, Chemsystems Perp Progr. (2013).

[3] E. V. Makshina, M. Dusselier, W. Janssens, J. Degrève, P.A. Jacobs, B.F. Sels, Review of old chemistry and new catalytic advances in the on-purpose synthesis of butadiene, Chem. Soc. Rev. 43 (2014) 7917–7953. doi:10.1039/C4CS00105B.

[4] European Commission, Going climate-neutral by 2050, Facilities. (2018).

[5] European Commission, A clean planet for all. A European strategic long-term vision for a prosperous, modern, competitive and climate neutral economy, (2018).

[6] R.G. Grim, A.T. To, C.A. Farberow, J.E. Hensley, D.A. Ruddy, J.A. Schaidle, Growing the Bioeconomy through Catalysis: A Review of Recent Advancements in the Production of Fuels and Chemicals from Syngas-Derived Oxygenates, ACS Catal. 9 (2019) 4145–4172. doi:10.1021/acscatal.8b03945.

[7] S. Shylesh, A.A. Gokhale, C.R. Ho, A.T. Bell, Novel Strategies for the Production of Fuels, Lubricants, and Chemicals from Biomass, Acc. Chem. Res. 50 (2017) 2589–2597. doi:10.1021/acs.accounts.7b00354.

[8] R.A. Sheldon, Green and sustainable manufacture of chemicals from biomass: state of the art, Green Chem. 16 (2014) 950–963. doi:10.1039/C3GC41935E.

[9] R.A. Flach B., Lieberz A., EU Annual Biofuels Annual 2017, USDA Foreign Agric. Serv. (2017).

[10] G. Pomalaza, M. Capron, V. Ordomsky, F. Dumeignil, Recent Breakthroughs in the Conversion of Ethanol to Butadiene, Catalysts. 6 (2016) 203. doi:10.3390/catal6120203.

[11] G. Pomalaza, P. Arango Ponton, M. Capron, F. Dumeignil, Ethanol-to-butadiene: The reaction and its catalysts, Catal. Sci. Technol. 10 (2020) 4860–4911. doi:10.1039/d0cy00784f.

[12] V. Gruver, A. Sun, J.J. Fripiat, Catalytic properties of aluminated sepiolite in ethanol conversion, Catal. Letters. 34 (1995) 359–364. doi:10.1007/BF00806885.

[13] A. Chieregato, J.V. Ochoa, C. Bandinelli, G. Fornasari, F. Cavani, M. Mella, On the chemistry of ethanol on basic oxides: Revising mechanisms and intermediates in the lebedev and guerbet reactions, ChemSusChem. 8 (2015) 377–388. doi:10.1002/cssc.201402632.

[14] J.V. Ochoa, C. Bandinelli, O. Vozniuk, A. Chieregato, A. Malmusi, C. Recchi, F. Cavani, An analysis of the chemical, physical and reactivity features of MgO–SiO_2 catalysts for butadiene synthesis with the Lebedev process, Green Chem. 18 (2016) 1653–1663. doi:10.1039/C5GC02194D.

[15] W.E. Taifan, T. Bučko, J. Baltrusaitis, Catalytic conversion of ethanol to 1,3-butadiene on MgO A comprehensive mechanism elucidation using DFT calculations.pdf, J. Catal. 346 (2017) 78–91. doi:10.1016/j.jcat.2016.11.042.

[16] W.E. Taifan, G.X. Yan, J. Baltrusaitis, Surface chemistry of MgO/SiO2catalyst during the ethanol catalytic conversion to 1,3-butadiene: In-situ DRIFTS and DFT study, Catal. Sci. Technol. 7 (2017) 4648–4668. doi:10.1039/c7cy01556a.

[17] L. Qi, Y. Zhang, M.A. Conrad, C.K. Russell, J. Miller, A.T. Bell, Ethanol Conversion to Butadiene over Isolated Zinc and Yttrium Sites Grafted onto Dealuminated Beta Zeolite, J. Am. Chem. Soc. 142 (2020) 14674–14687. doi:10.1021/jacs.0c06906.

[18] S. Bhattacharyya, Kinetic study on the mechanism of the catalytic conversion of ethanol to butadiene, J. Catal. 7 (1967) 152–158. doi:10.1016/0021-9517(67)90053-X.

[19] M. Gao, Z. Liu, M. Zhang, L. Tong, Study on the mechanism of butadiene formation from ethanol, Catal. Letters. 144 (2014) 2071–2079. doi:10.1007/s10562-014-1370-x.

[20] W. Janssens, E. V. Makshina, P. Vanelderen, F. De Clippel, K. Houthoofd, S. Kerkhofs, J.A. Martens, P.A. Jacobs, B.F. Sels, Ternary Ag/MgO-SiO $_2$ Catalysts for the Conversion of Ethanol into Butadiene, ChemSusChem. 8 (2015) 994–1008. doi:10.1002/cssc.201402894.

[21] M.D. Jones, Catalytic transformation of ethanol into 1,3-butadiene, Chem. Cent. J. 8 (2014) 1–5. doi:10.1186/s13065-014-0053-4.

[22] G. Natta, R. Rigamonti, Synthesis of butadiene from ethyl alcohol. Thermodynamic studies and the specific function of catalysts, Chim. Ind. 29 (1947) 195–200.

[23] V.L. Sushkevich, I.I. Ivanova, V. V. Ordomsky, E. Taarning, Design of a Metal-Promoted Oxide Catalyst for the Selective Synthesis of Butadiene from Ethanol, ChemSusChem. 7 (2014) 2527–2536. doi:10.1002/cssc.201402346.

[24] V.L. Sushkevich, I.I. Ivanova, S. Tolborg, E. Taarning, Meerwein-Ponndorf-Verley-Oppenauer reaction of crotonaldehyde with ethanol over Zr-containing catalysts, J. Catal. 316 (2014) 121–129. doi:10.1016/j.jcat.2014.04.019.

[25] V.F. Tret'yakov, R.M. Talyshinskii, A.M. Ilolov, A.L. Maksimov, S.N. Khadzhiev, Initiated conversion of ethanol to divinyl by the lebedev reaction, Pet. Chem. 54 (2014) 195–206. doi:10.1134/S0965544114020133.

[26] G.O. Ezinkwo, V.F. Tretjakov, R.M. Talyshinky, A.M. Ilolov, T.A. Mutombo, Creation of a continuous process for bio-ethanol to butadiene conversion via the use of a process initiator, Catal. Commun. 43 (2014) 207–212. doi:10.1016/j.catcom.2013.10.015.

[27] V.S. Bharadwaj, M.B. Pecha, L. Bu, V.L. Dagle, R.A. Dagle, P.N. Ciesielski, Multi-scale

simulation of reaction, transport and deactivation in a SBA-16 supported catalyst for the conversion of ethanol to butadiene, Catal. Today. 338 (2019) 141–151. doi:10.1016/j.cattod.2019.05.042.

[28] A. Talalay, L. Talalay, S.K.-The Russian Synthetic Rubber From Alcohol - A Survey of the Chemistry and Technology of the Lebedev Process for Producing Sodium-Butadiene Polymers, Rubber Chem. Technol. 15 (1942) 403–429. http://rubberchemtechnol.org/doi/pdf/10.5254/1.3543128.

[29] P.I. Kyriienko, O. V Larina, S. Dzwigaj, S.O. Soloviev, S.M. Orlyk, Effect of the Composition of Ethanol–Water Mixtures on the Properties of Oxide (Zn-Zr-Si) and Zeolitic (Ta/SiBEA) Catalysts in the Production of 1,3-Butadiene, Theor. Exp. Chem. 55 (2019) 266–273. doi:10.1007/s11237-019-09618-1.

[30] O. V. Larina, I.M. Remezovskyi, P.I. Kyriienko, S.O. Soloviev, S.M. Orlyk, 1,3-Butadiene production from ethanol–water mixtures over Zn–La–Zr–Si oxide catalyst, React. Kinet. Mech. Catal. 127 (2019) 903–915. doi:10.1007/s11144-019-01618-5.

[31] P.I. Kyriienko, O. V. Larina, S.O. Soloviev, S.M. Orlyk, Catalytic Conversion of Ethanol Into 1,3-Butadiene: Achievements and Prospects: A Review, Theor. Exp. Chem. 56 (2020) 213–242. doi:10.1007/s11237-020-09654-2.

[32] O. V Larina, N.D. Shcherban, P.I. Kyriienko, I.M. Remezovskyi, P.S. Yaremov, I. Khalakhan, G. Mali, S.O. Soloviev, S.M. Orlyk, S. Dzwigaj, Design of Effective Catalysts Based on ZnLaZrSi Oxide Systems for Obtaining 1,3-Butadiene from Aqueous Ethanol, ACS Sustain. Chem. Eng. 8 (2020) 16600–16611. doi:10.1021/acssuschemeng.0c05925.

[33] G.M. Cabello González, P. Concepción, A.L. Villanueva Perales, A. Martínez, M. Campoy, F. Vidal-Barrero, Ethanol conversion into 1,3-butadiene over a mixed Hf-Zn catalyst: Effect of reaction conditions and water content in ethanol, Fuel Process. Technol. 193 (2019) 263–272. doi:10.1016/j.fuproc.2019.04.036.

[34] C.E. Cabrera Camacho, B. Alonso-Fariñas, A.L. Villanueva Perales, F. Vidal-Barrero, P. Ollero, Techno-economic and Life-Cycle Assessment of One-Step Production of 1,3-Butadiene from Bioethanol Using Reaction Data under Industrial Operating Conditions, ACS Sustain. Chem. Eng. (2020). doi:10.1021/acssuschemeng.0c02678.

[35] G.M. Cabello González, R. Murciano, A.L. Villanueva Perales, A. Martínez, F. Vidal-Barrero, M. Campoy, Ethanol conversion into 1,3-butadiene over a mixed Hf-Zn catalyst: A study of the reaction pathway and catalyst deactivation, Appl. Catal. A Gen. 570 (2019) 96–106. doi:10.1016/j.apcata.2018.11.010.

[36] C. Angelici, B.M. Weckhuysen, P.C.A. Bruijnincx, Chemocatalytic conversion of ethanol into butadiene and other bulk chemicals, ChemSusChem. 6 (2013) 1595–1614. doi:10.1002/cssc.201300214.

[37] T. Riittonen, T. Salmi, J.P. Mikkola, J. Wärnå, Direct Synthesis of 1-Butanol from Ethanol in a Plug Flow Reactor: Reactor and Reaction Kinetics Modeling, Top. Catal. 57 (2014) 1425–1429. doi:10.1007/s11244-014-0314-4.

[38] T. Yan, L. Yang, W. Dai, C. Wang, G. Wu, N. Guan, M. Hunger, L. Li, On the deactivation mechanism of zeolite catalyst in ethanol to butadiene conversion, J. Catal. 367 (2018) 7–15. doi:10.1016/J.JCAT.2018.08.019.

[39] A.G. Gayubo, A.M. Tarrío, A.T. Aguayo, M. Olazar, J. Bilbao, Kinetic modelling of the transformation of aqueous ethanol into hydrocarbons on a HZSM-5 zeolite, Ind. Eng. Chem. Res. 40 (2001) 3467–3474. doi:10.1021/ie001115e.

[40] C.D. Knightes, C.A. Peters, Statistical analysis of nonlinear parameter estimation for Monod biodegradation kinetics using bivariate data, Biotechnol. Bioeng. 69 (2000) 160–170. doi:10.1002/(SICI)1097-0290(20000720)69:2<160::AID-BIT5>3.0.CO;2-J.

[41] F.D. Marques-Marinho, I.A. Reis, C.D. Vianna-Soares, Construction of analytical curve fit models for simvastatin using ordinary and weighted least squares methods, J. Braz. Chem. Soc. 24 (2013) 1469–1477. doi:10.5935/0103-5053.20130187.

[42] H.S. Fogler, Elements of chemical reaction engineering. 6th ed, Prentice Hall, 2020.

[43] M.A. Portillo, A.L.V. Perales, F. Vidal-Barrero, M. Campoy, A kinetic model for the synthesis of ethanol from syngas and methanol over an alkali-Co doped molybdenum sulfide catalyst: Model building and validation at bench scale, Fuel Process. Technol. 151 (2016) 19–30. doi:10.1016/j.fuproc.2016.05.027.

[44] Y. Bard, Nonlinear parameter estimation, Academic Press, New York, 1974.

[45] N.R. Draper, H. Smith, Applied regression analysis, John Wiley & Sons, 1998.

Supporting information for:

Kinetic modelling of the one-step conversion of aqueous ethanol into 1,3-butadiene over a mixed hemimorphite-HfO_2/SiO_2 catalyst

G. M. Cabello González[1], A. L. Villanueva Perales[1*], M. Campoy[1], J. R. López Beltran[1], A. Martínez[2], F. Vidal-Barrero[1]

[1]Departamento de Ingeniería Química y Ambiental, Escuela Técnica Superior de Ingeniería, Universidad de Sevilla, Camino de los Descubrimientos, s/n. 41092 Sevilla, Spain.

[2]Instituto de Tecnología Química, Universitat Politècnica de València-Consejo Superior de Investigaciones Científicas (UPV-CSIC), Avda. de los Naranjos s/n, 46022 Valencia, Spain.

* Corresponding author
email: angelluisvp@us.es
Departamento de Ingeniería Química y Ambiental, Escuela Técnica Superior de Ingeniería, Universidad de Sevilla, Camino de los Descubrimientos, s/n. 41092 Sevilla, Spain.

Appendix A. Operation conditions and results of the catalytic test used for estimation and validation of the kinetic model

Table A.1. *Operating condition and inlet flow rates. Total pressure is 1 bar. WHSV is defined as mass flow rate of ethanol feed (water-free) divided by catalyst load*

Test	Catalyst load (g)	WHSV (h^{-1})	T (ºC)	Mole flow (mol/h)		
				Ethanol	Nitrogen	Water
1	1.0	1.12	360	0.0243	0.0911	-
2	1.0	1.87	360	0.0407	0.1527	-
3	1.0	3.73	360	0.0811	0.3027	-
4	1.0	1.87	360	0.0407	0.1527	-
5	1.0	1.12	360	0.0243	0.0911	-
6	1.0	1.87	360	0.0407	0.1527	-
7	0.5	5.60	360	0.0609	0.2277	-
8	0.5	11.20	360	0.1217	0.4554	-
9	0.5	5.60	360	0.0609	0.2277	-
10	0.5	11.20	360	0.1217	0.4554	-
11	0.5	5.60	360	0.0609	0.2277	-
12	0.5	3.73	360	0.0405	0.1527	-
13	0.5	7.00	360	0.0761	0.2839	-
14	0.1	11.20	360	0.0243	0.0911	-
15	0.1	30.00	360	0.0652	0.2438	-
16	0.1	50.00	360	0.1087	0.4071	-
17	2.0	1.12	360	0.0487	0.1821	-
18	2.0	1.12	360	0.0487	0.1821	-
19	0.5	9.80	340	0.1065	0.3964	-
20	0.5	6.10	340	0.0663	0.2464	-
21	0.5	3.20	340	0.0348	0.1286	-
22	0.5	1.12	340	0.0122	0.0455	-
23	0.5	9.80	360	0.1065	0.3964	-
24	0.5	6.10	360	0.0663	0.2464	-
25	0.5	3.20	360	0.0348	0.1286	-
26	0.5	1.12	360	0.0122	0.0455	-
27	0.5	9.80	380	0.1065	0.3964	-
28	0.5	6.10	380	0.0663	0.2464	-
29	0.5	3.20	380	0.0348	0.1286	-
30	0.5	1.12	380	0.0122	0.0455	-
31	1.0	8.00	340	0.0870	0.3054	0.0183
32	1.0	6.10	340	0.0663	0.2330	0.0139
33	1.0	3.20	340	0.0348	0.1232	0.0072
34	1.0	1.12	340	0.0122	0.0429	0.0028
35	1.0	8.00	340	0.0870	0.2866	0.0394
36	1.0	6.10	340	0.0663	0.2196	0.0300
37	0.5	3.20	340	0.0348	0.1152	0.0156
38	0.5	1.12	340	0.0122	0.0402	0.0056
39	0.5	8.00	360	0.0870	0.3080	0.0020
40	0.5	6.10	360	0.0663	0.2357	0.0016
41	0.5	3.20	360	0.0348	0.1232	0.0008
42	0.5	1.12	360	0.0122	0.0429	0.0003
43	0.5	8.00	360	0.0870	0.3054	0.0183
44	0.1	6.10	360	0.0663	0.2330	0.0139
45	0.1	3.20	360	0.0348	0.1232	0.0072
46	0.1	1.12	360	0.0122	0.0429	0.0028
47	2.0	8.00	360	0.0870	0.2866	0.0394
48	2.0	6.10	360	0.0663	0.2196	0.0300
49	0.5	3.20	360	0.0348	0.1152	0.0156
50	0.5	1.12	360	0.0122	0.0402	0.0056
51	0.5	8.00	380	0.0870	0.3054	0.0183
52	0.5	6.10	380	0.0663	0.2330	0.0139
53	0.5	3.20	380	0.0348	0.1232	0.0072
54	0.5	1.12	380	0.0122	0.0429	0.0028
55	0.5	8.00	380	0.0870	0.2866	0.0394
56	0.5	6.10	380	0.0663	0.2196	0.0300
57	0.5	3.20	380	0.0348	0.1152	0.0156
58	0.5	1.12	380	0.0122	0.0402	0.0056

Table A.2. *Mole flow rates at the reactor outlet. BD=1,3-butadiene, Ac=acetaldehyde, C4=butenes, BuOH=1-butanol, Et=ethene, C_{6+}=heavy compounds, DEE=diethyl ether, Oc=oxygenated compounds, EtOH=ethanol.*

Test	Mole flow (mol/h)										
	BD	**Ac**	**C_4**	**BuOH**	**Et**	**C_{6+}**	**DEE**	**Oc**	**EtOH**	**H_2O**	**H_2**
1	0.0045	0.0016	0.0005	0.0000	0.0009	0.0007	0.0001	0.0019	0.0032	0.0168	0.0143
2	0.0067	0.0046	0.0006	0.0001	0.0012	0.0008	0.0002	0.0023	0.0099	0.0228	0.0206
3	0.0114	0.0130	0.0009	0.0004	0.0017	0.0010	0.0004	0.0035	0.0265	0.0362	0.0370
4	0.0074	0.0051	0.0007	0.0001	0.0012	0.0009	0.0002	0.0023	0.0073	0.0248	0.0226
5	0.0046	0.0014	0.0004	0.0001	0.0009	0.0008	0.0001	0.0018	0.0031	0.0171	0.0148
6	0.0061	0.0038	0.0005	0.0001	0.0009	0.0010	0.0002	0.0028	0.0102	0.0226	0.0215
7	0.0064	0.0109	0.0004	0.0003	0.0009	0.0005	0.0002	0.0030	0.0250	0.0209	0.0249
8	0.0086	0.0265	0.0006	0.0006	0.0014	0.0006	0.0003	0.0040	0.0614	0.0283	0.0449
9	0.0077	0.0109	0.0006	0.0004	0.0010	0.0006	0.0002	0.0031	0.0214	0.0243	0.0268
10	0.0089	0.0262	0.0007	0.0007	0.0014	0.0007	0.0003	0.0038	0.0609	0.0291	0.0449
11	0.0068	0.0114	0.0005	0.0004	0.0010	0.0005	0.0002	0.0029	0.0240	0.0216	0.0254
12	0.0045	0.0066	0.0003	0.0002	0.0006	0.0005	0.0001	0.0022	0.0152	0.0156	0.0179
13	0.0064	0.0148	0.0005	0.0005	0.0009	0.0009	0.0002	0.0029	0.0334	0.0234	0.0322
14	0.0014	0.0044	0.0001	0.0001	0.0002	0.0002	0.0000	0.0008	0.0137	0.0052	0.0082
15	0.0018	0.0110	0.0003	0.0002	0.0006	0.0002	0.0001	0.0013	0.0453	0.0072	0.0156
16	0.0011	0.0181	0.0003	0.0002	0.0005	0.0001	0.0001	0.0011	0.0841	0.0051	0.0212
17	0.0090	0.0033	0.0008	0.0001	0.0017	0.0014	0.0003	0.0033	0.0076	0.0327	0.0280
18	0.0085	0.0033	0.0007	0.0001	0.0014	0.0015	0.0003	0.0029	0.0095	0.0312	0.0279
19	0.0057	0.0153	0.0004	0.0004	0.0012	0.0002	0.0003	0.0017	0.0715	0.0171	0.0248
20	0.0052	0.0100	0.0004	0.0003	0.0009	0.0002	0.0002	0.0016	0.0387	0.0152	0.0183
21	0.0041	0.0043	0.0003	0.0002	0.0007	0.0002	0.0002	0.0014	0.0164	0.0123	0.0114
22	0.0017	0.0009	0.0002	0.0000	0.0004	0.0002	0.0001	0.0010	0.0037	0.0063	0.0052
23	0.0107	0.0185	0.0008	0.0005	0.0019	0.0004	0.0003	0.0035	0.0518	0.0315	0.0364
24	0.0085	0.0112	0.0007	0.0003	0.0015	0.0003	0.0002	0.0028	0.0263	0.0251	0.0256
25	0.0058	0.0057	0.0005	0.0001	0.0011	0.0002	0.0002	0.0017	0.0101	0.0168	0.0151
26	0.0024	0.0010	0.0003	0.0000	0.0006	0.0002	0.0001	0.0010	0.0016	0.0083	0.0064
27	0.0152	0.0201	0.0013	0.0004	0.0032	0.0006	0.0004	0.0046	0.0355	0.0450	0.0455
28	0.0107	0.0126	0.0010	0.0002	0.0022	0.0006	0.0002	0.0041	0.0150	0.0336	0.0330
29	0.0054	0.0048	0.0005	0.0001	0.0011	0.0011	0.0001	0.0032	0.0035	0.0221	0.0229
30	0.0015	0.0011	0.0002	0.0000	0.0004	0.0006	0.0000	0.0013	0.0006	0.0086	0.0094
31	0.0026	0.0136	0.0002	0.0001	0.0011	0.0001	0.0003	0.0004	0.0649	0.0260	0.0170
32	0.0030	0.0123	0.0002	0.0001	0.0012	0.0001	0.0003	0.0005	0.0442	0.0227	0.0164
33	0.0031	0.0064	0.0002	0.0001	0.0010	0.0001	0.0002	0.0004	0.0189	0.0159	0.0105
34	0.0018	0.0014	0.0002	0.0000	0.0007	0.0000	0.0001	0.0003	0.0049	0.0081	0.0039
35	0.0021	0.0139	0.0001	0.0001	0.0013	0.0000	0.0003	0.0003	0.0656	0.0461	0.0167
36	0.0022	0.0121	0.0001	0.0001	0.0012	0.0000	0.0003	0.0003	0.0469	0.0366	0.0148
37	0.0021	0.0058	0.0001	0.0001	0.0009	0.0000	0.0002	0.0002	0.0226	0.0215	0.0083
38	0.0016	0.0016	0.0001	0.0000	0.0007	0.0000	0.0001	0.0002	0.0055	0.0102	0.0036
39	0.0070	0.0169	0.0004	0.0002	0.0021	0.0001	0.0004	0.0012	0.0486	0.0214	0.0261
40	0.0063	0.0128	0.0004	0.0002	0.0019	0.0001	0.0003	0.0011	0.0342	0.0191	0.0212
41	0.0056	0.0059	0.0005	0.0001	0.0018	0.0001	0.0003	0.0013	0.0109	0.0170	0.0137
42	0.0025	0.0015	0.0003	0.0000	0.0009	0.0001	0.0001	0.0007	0.0022	0.0079	0.0052
43	0.0067	0.0171	0.0004	0.0002	0.0020	0.0001	0.0004	0.0014	0.0489	0.0372	0.0263
44	0.0058	0.0140	0.0004	0.0002	0.0018	0.0001	0.0003	0.0012	0.0341	0.0303	0.0218
45	0.0045	0.0067	0.0004	0.0001	0.0014	0.0001	0.0002	0.0009	0.0139	0.0200	0.0128
46	0.0023	0.0016	0.0003	0.0000	0.0009	0.0001	0.0001	0.0006	0.0027	0.0099	0.0050
47	0.0054	0.0200	0.0003	0.0002	0.0024	0.0001	0.0005	0.0009	0.0493	0.0554	0.0273
48	0.0048	0.0151	0.0003	0.0002	0.0021	0.0001	0.0004	0.0008	0.0359	0.0439	0.0212
49	0.0042	0.0074	0.0003	0.0001	0.0017	0.0001	0.0003	0.0007	0.0141	0.0277	0.0128
50	0.0023	0.0018	0.0002	0.0000	0.0011	0.0000	0.0001	0.0006	0.0025	0.0127	0.0050
51	0.0116	0.0207	0.0008	0.0003	0.0035	0.0002	0.0005	0.0025	0.0304	0.0508	0.0365
52	0.0102	0.0164	0.0008	0.0002	0.0031	0.0002	0.0004	0.0022	0.0183	0.0425	0.0303
53	0.0068	0.0078	0.0006	0.0001	0.0022	0.0001	0.0002	0.0017	0.0052	0.0269	0.0174
54	0.0029	0.0014	0.0003	0.0000	0.0010	0.0002	0.0001	0.0009	0.0004	0.0121	0.0065
55	0.0111	0.0218	0.0007	0.0003	0.0039	0.0002	0.0005	0.0021	0.0307	0.0709	0.0369
56	0.0091	0.0173	0.0006	0.0002	0.0032	0.0002	0.0004	0.0017	0.0205	0.0560	0.0297
57	0.0067	0.0080	0.0006	0.0001	0.0025	0.0001	0.0002	0.0015	0.0054	0.0351	0.0172
58	0.0028	0.0018	0.0003	0.0000	0.0012	0.0001	0.0001	0.0009	0.0002	0.0146	0.0066

Appendix B. Residual analysis and model validation

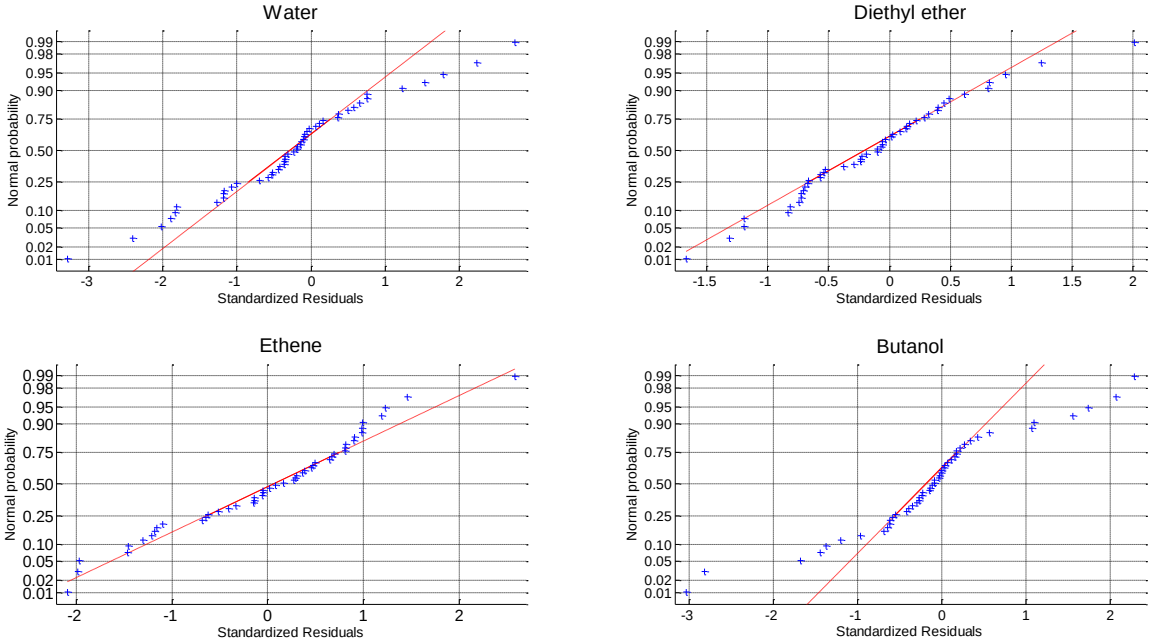

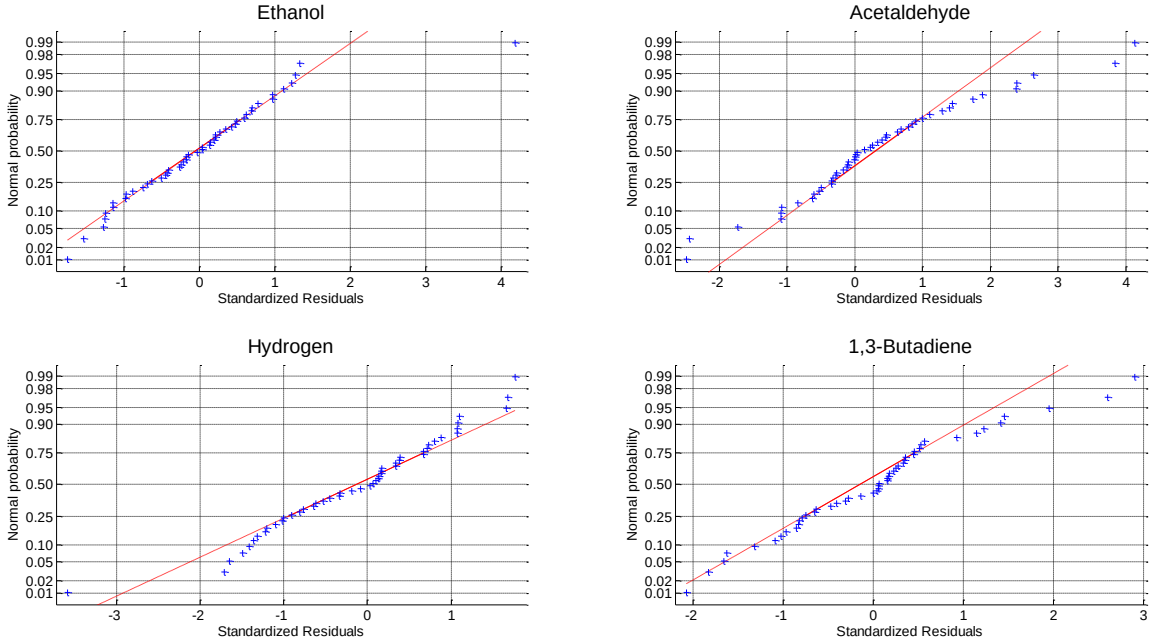

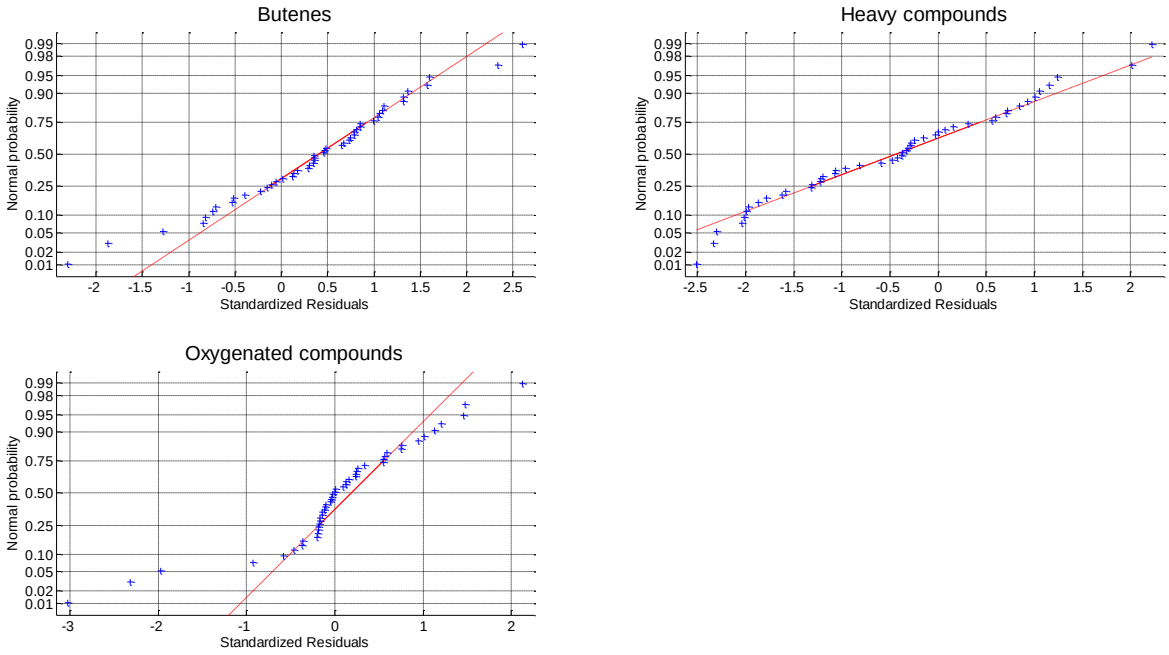

721

722 Figure B.1. Normal distribution of standardized residuals for the estimation data

723

724

725

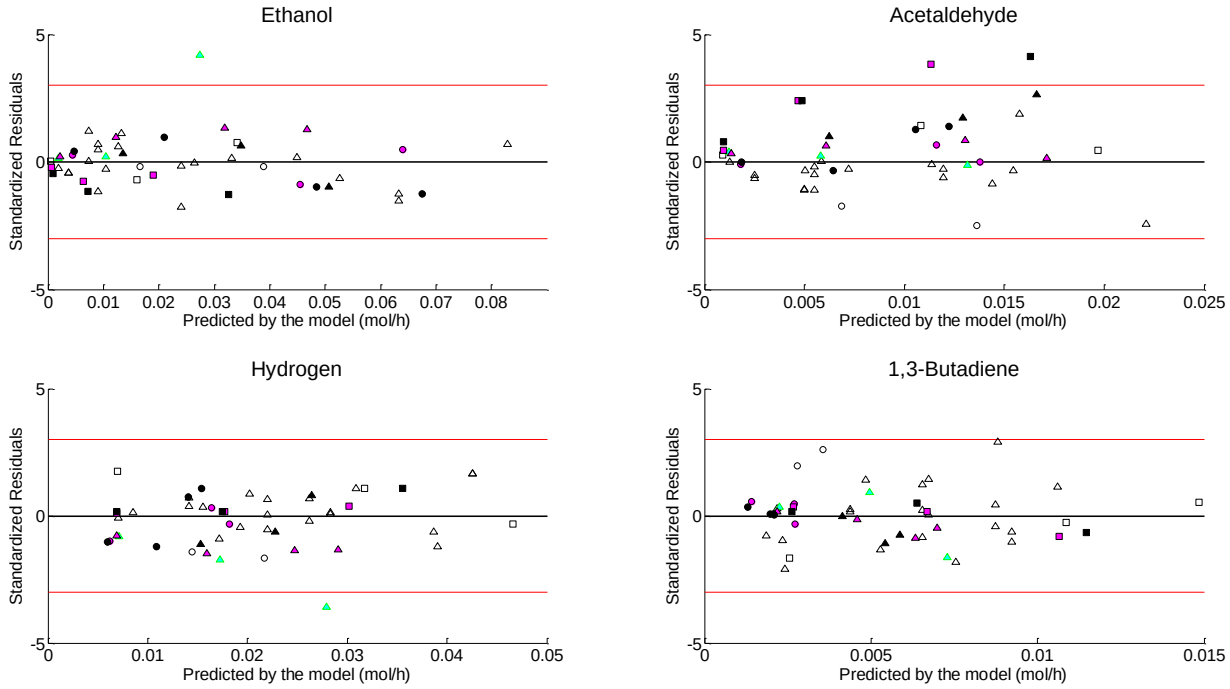
Ethanol
Acetaldehyde
Hydrogen
1,3-Butadiene
Standardized Residuals
Predicted by the model (mol/h)

726

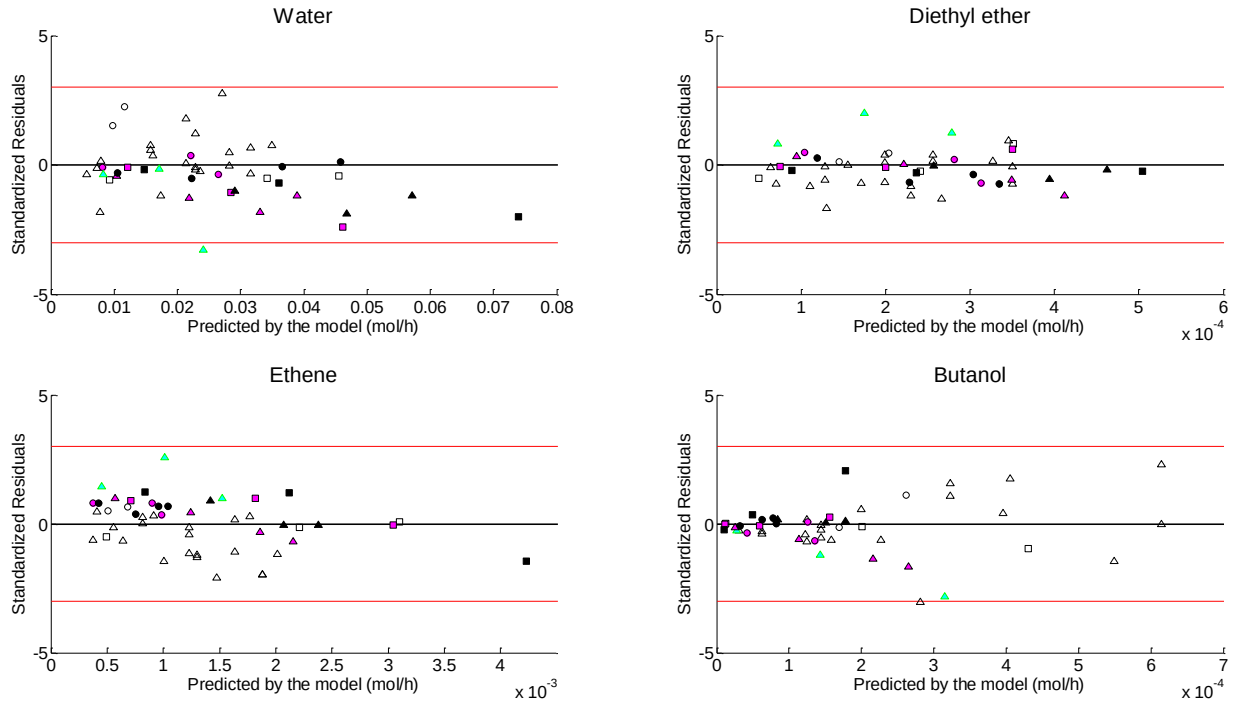
Water
Diethyl ether
Ethene
Butanol
Standardized Residuals
Predicted by the model (mol/h)
x 10^-4
x 10^-3

727

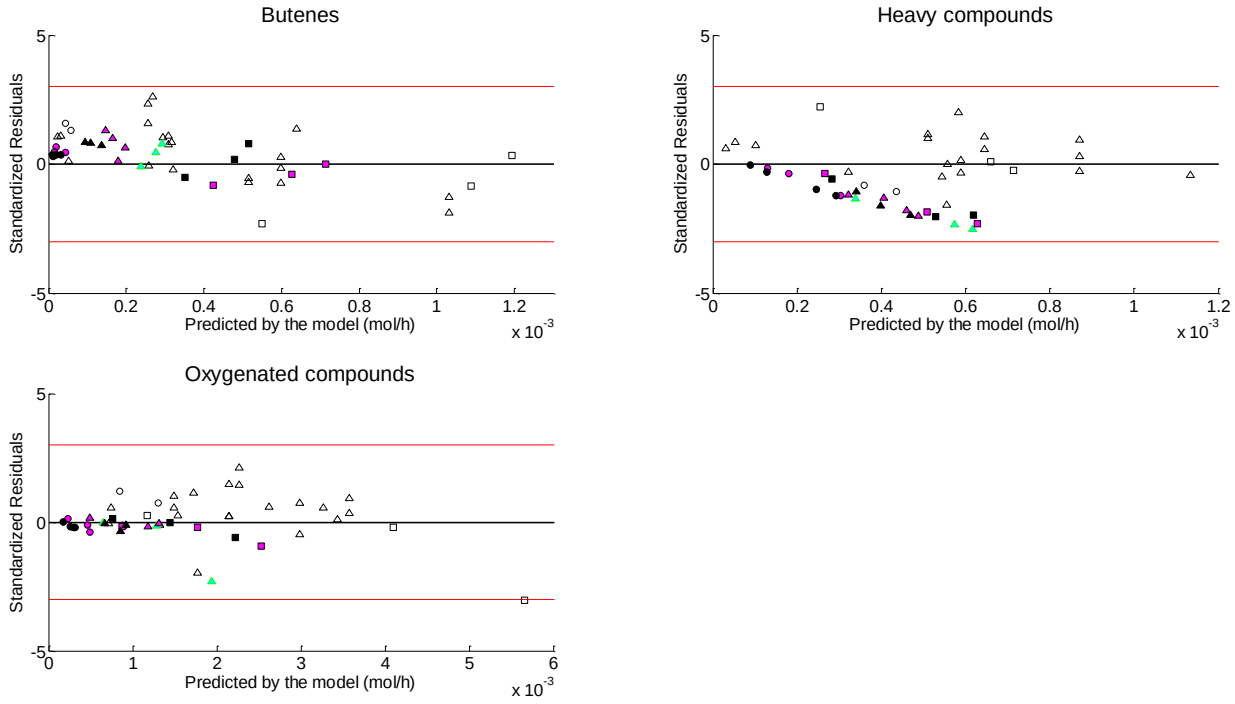

Figure B.2**.** Standardized residuals versus predicted values for estimation data. Temperature of experiments 340°C (circle), 360°C (triangle) and 380°C (square). Water content in ethanol feed: blank: 0 wt%, cyan: 3.75 wt%, magenta: 7.5 wt%, black: 15 wt%).

Appendix C. Estimation of the internal and external mass transfer limitation in the catalytic tests

An evaluation of the possible external and internal diffusion limitation was assessed to check out that the chemical reaction was the rate-controlling step for each reaction. For every catalytic test, Mears criterion was applied to all reactions to evaluate the influence of external mass transfer effects. This criterion states that external mass transport limitations can be neglected in case the Mears number (C_{Mears}) is under 0.15 [1]. C_{Mears} number is defined in Equation C1, where $-r_{obs}$ is the observed reaction rate (kmol/kg·s), ρ_c is the density of catalyst (kg/m^3), d_p is the diameter of the pellets ($5 \cdot 10^{-4}$ m), n_k is the reaction order of reactant *k*, k_c is the mass transfer coefficient (m/s), and C_k the concentration of the reactant *k* in the bulk gas phase (kmol/m^3).

$$C_{Mears} = \frac{-r_{obs} \cdot \rho_c \cdot d_p \cdot n_k}{2 \cdot k_c \cdot C_k} \qquad \text{Equation C1}$$

To determine whether internal diffusion is limiting the reaction, the Weisz-Prater criterion was employed [2]. The Weisz-Prater number (C_{WP}) relates the observed reaction rate with the diffusion rate, so if C_{WP} is lower than 0.15 there are no diffusion limitations and, consequently, no concentration gradient exists within the catalytic pellets. C_{WP} number is defined in Equation C2, where D_e is the effective diffusion coefficient in the pores of the catalyst (m^2/s), and C_{kS} is the concentration of the reactant *k* on the catalyst surface (kmol/m^3).

$$C_{WP} = \frac{-r_{obs} \cdot \rho_c \cdot (d_p/2)^2}{D_e \cdot C_{kS}} \qquad \text{Equation C2}$$

Both the C_{Mears} and C_{WP} were evaluated at the reactor outlet for each catalytic test. The obtained C_{Mears} values were around $2 \cdot 10^{-3}$, which is far below 0.15 and confirms that, for all the catalytic tests, no concentration gradient exists between the bulk gas and the external surface of the catalyst particle (external diffusion negligible). Also, the calculated C_{WP} values were around $1 \cdot 10^{-5}$, which is much lower than 0.15, confirming that internal diffusion was negligible too.

[1] Mears D.E. Tests for transport limitations in experimental catalytic reactors. Ind. Eng. Chem. Process Des. Develop., 10 (1971), 541-547.

[2] Weisz PB, Prater CD. Interpretation of Measurements in Experimental Catalysis. Advances in Catalysis, 6 (1954), 143-196.